Research article

Yuanhai Lin, Thanh Xuan Hoang, Hong-Son Chu* and Christian A. Nijhuis*

Directional launching of surface plasmon polaritons by electrically driven aperiodic groove array reflectors

https://doi.org/10.1515/nanoph-2020-0558
Received October 4, 2020; accepted December 2, 2020; published online December 14, 2020

Abstract: Access to surface plasmon polaritons (SPPs) with directional control excited by electrical means is important for applications in (on-chip) nano-optoelectronic devices and to circumvent limitations inherent to approaches where SPPs are excited by optical means (e.g., diffraction limit). This paper describes directional excitation of surface plasmon polaritons propagating along a plasmonic strip waveguide integrated with an aperiodic groove array electrically driven by an Al–Al_2O_3–Au tunnel junction. The aperiodic groove array consists of six grooves and is optimized to specifically reflect the SPPs by 180° in the desired direction ($+x$ or $-x$) along the plasmonic strip waveguide. We used constrained nonlinear optimization of the groove array based on the sequential quadratic programming algorithms coupled with finite-difference time-domain (FDTD) simulations to achieve the optimal structures. Leakage radiation microscopy (Fourier and real plane imaging) shows that the propagation direction of selectively only one SPP mode (propagating along the metal–substrate interface) is controlled. In our experiments, we achieved a directionality (i.e., $+x/-x$ ratio) of close to 8, and all of our experimental findings are supported by detailed theoretical simulations.

Keywords: aperiodic groove array; electrical excitation; plasmon launching; surface plasmon polaritons; tunnel junction.

1 Introduction

Surface plasmon polaritons (SPPs) confine electromagnetic fields at dielectric–metal interfaces [1] and are promising candidates for applications in subwavelength imaging [2], sensing [3], and other areas in nanotechnology [4–6], because of strong field enhancement and their capability to overcome the diffraction limit [7]. Usually, SPPs are excited by optical means using, for instance, lasers and prisms or simple gratings, but such approaches using external light sources are diffraction limited and normally do not provide control over the propagation direction of the SPPs [8]. Directional excitation of SPPs by optical means has been achieved in plasmonic structures such as asymmetric (slot) nanoantennae [9, 10], aperiodic gratings [11, 12], or Bragg mirrors [13]. For many applications, however, especially in nano-optoelectronics [14] or sensing [15], directional control over the propagation of SPPs excited by electrical means is needed. We demonstrate, for the first time, unidirectional SPP excitation along a plasmonic waveguide from an aperiodic groove array (designed to reflect propagating SPPs by 180°) electrically driven by a quantum mechanical tunnel junction.

It is well-known that SPPs and photons in free space can be electrically excited via inelastic quantum mechanical tunneling in metal–insulator–metal tunnel junctions (MIM-TJs) [16–20]. Direct excitation of plasmons by tunneling electrons is attractive because the process occurs at tunneling time scales on the order of fs [21], which is much faster than electron–hole recombination processes (>1 ps) for photon generation [22]. Theoretical models predict internal excitation efficiencies of 10% [23], so far the highest reported external efficiencies of SPPs and photons

***Corresponding authors: Hong-Son Chu**, Department of Electronics and Photonics, Institute of High Performance Computing, A*STAR (Agency for Science, Technology and Research), 1 Fusionopolis Way, #16-16 Connexis, Singapore 138632, Singapore; and **Christian A. Nijhuis**, Centre for Advanced 2D Materials, National University of Singapore, 6 Science Drive 2, Singapore 117543, Singapore; and Department of Chemistry, National University of Singapore, 3 Science Drive 3, Singapore 117543, Singapore, E-mail: chuhs@ihpc.a-star.edu.sg (H.-S. Chu), chmnca@nus.edu.sg (C. A. Nijhuis). https://orcid.org/0000-0003-3435-4600
Yuanhai Lin, Centre for Advanced 2D Materials, National University of Singapore, 6 Science Drive 2, Singapore 117543, Singapore
Thanh Xuan Hoang, Department of Electronics and Photonics, Institute of High Performance Computing, A*STAR (Agency for Science, Technology and Research), 1 Fusionopolis Way, #16-16 Connexis, Singapore 138632, Singapore

generated by MIM-TJs are 1–2% [20, 24]. These efficiencies are high enough to drive and modulate optical antennae [25–29]. Such systems have been used to demonstrate directional light emission of photons in free space [30, 31], but directional control over SPPs excited by MIM-TJs has not been demonstrated. We note that MIM-TJs are commercially available (e.g., magnetic tunnel junctions, Josephson junctions, tunnel diodes, millimeter wave detectors, or rectennas) [32–36] and can be scaled to sub-hundred nanometers [37, 38]. The challenge is to outcouple the highly confined MIM SPP mode to a single interface SPP mode that propagates along a dielectric–metal interface of a plasmonic waveguide because the momentum of the MIM SPP is one order of magnitude larger than that of the single interface SPPs [39–41].

Aperiodic groove arrays have been used for directional launching of SPPs excited by incident laser light (often along the surface normal) and make it possible to design compact optical elements [11, 12]. The SPP mode interacts with each groove resulting in interference with adjacent grooves, and hence the directionality—the ratio of SPP power flowing in the $+x$ and $-x$ directions—of the SPPs increases with increasing the groove numbers [42, 43]. An aperiodic grating consisting of 11 grooves with varying depth and width was optimized by the simplex search Nelder–Mead method and experimentally achieved the directionality of 47 [12]. To simplify fabrication, metallic groove array with the same depth but with different widths of, and distances between, the grooves was designed by gradient descent algorithm for the excitation of unidirectional SPPs with a directionality up to 55 [11]. However, such aperiodic structures have not been used as reflectors to alter the propagation directional of the SPPs, as we show here, by 180°-driven tunnel junctions.

This paper describes Al–Al_2O_3–Au junctions that were fabricated on glass substrates connected to a plasmonic strip waveguide. By controlling the thickness of the Al and Au electrodes, the outcoupling of the MIM SPP mode, to either the SPP mode propagating along the Au-glass, $SPP_{Au-glass}$, Au-air, SPP_{Au-air}, and Al-air interface, SPP_{Al-air}, can be controlled. Unlike excitation by optical means, high-order $SPP_{Au-glass}$ modes and one-dimensional edge modes can be readily excited in tunnel junction due to the large momentum of the tunneling charge carrier. We integrated an aperiodic groove array (based on a new and more efficient inverse design approach [44] which is an algorithmic technique to optimize optical structures) into the plasmonic waveguide; this array acts as a mirror to reflect the $SPP_{Au-glass}$ modes and, consequently, to control its directionality. By tuning the applied bias, we achieved voltage-dependent directionality of the excitation of the $SPP_{Au-glass}$ mode with a maximum value of 7.59 ± 0.93. We used finite-difference time-domain (FDTD) simulations to calculate the SPP modes excited by the tunnel junction and found that the $SPP_{Au-glass}$ mode was effectively reflected by the aperiodic groove array. The achievement of directional SPP excitation with electrically driven aperiodic groove array mitigates the need for external bulky optical elements opening up a pathway for on-chip control over SPPs.

2 The design of the junctions

Figure 1a shows schematically the tunnel junction consisting of a 90-nm-thick Al bottom electrode, 2–3 nm native Al_2O_3 tunnel barrier, and a 150-nm-thick Au top electrode which also serves as the plasmonic strip waveguide. By applying a bias across the tunnel junction, electrons inelastically tunneling through the insulator exciting MIM SPPs that are tightly confined within the metal–insulator–metal cavity (inset in Figure 1a). In this design, the 150-nm-thick top electrode is much (six times) thicker than the skin depth of SPPs and effectively blocks outcoupling of the MIM SPP mode to the SPP_{Au-air} modes [45]. The 90 nm thick Al electrode is about five times thicker than the skin depth of SPPs, and therefore we expect that the MIM SPP mode can only outcouple at the "edges" of the junctions, as indicated in Figure 1b, and excite the $SPP_{Au-glass}$ mode. Figure 1a indicates that the SPP_{Al-air} and SPP_{Au-air} modes also can be excited at the "corners" of the junction, albeit with lower efficiency than the metal-glass SPP mode (see below).

Figure 1 also indicates that SPPs propagating along the Au metal strip can propagate away from the junction along the plasmonic strip waveguide in either $-x$ (denoted as $SPP^-_{Au-glass}$) or $+x$ ($SPP^+_{Au-glass}$) directions, where $x = 0$ is at the center of the junction. To realize unidirectionality, we placed an aperiodic groove array consisting of six grooves integrated into the Au waveguide to reflect the $SPP^-_{Au-glass}$ mode by 180° to the $SPP^+_{Au-glass}$ direction as indicated in Figure 1a. Equation (1) defines the extinction ratio R_e to describe the directionality of $SPP_{Au-glass}$ propagation, where P^+ and P^- represent the SPP power (in W) flowing to the $+x$ and $-x$ directions.

$$R_e = \frac{P^+}{P^-} \tag{1}$$

The junction depicted in Figure 1a is inherently asymmetric; therefore, we also fabricated a symmetrical junction depicted in Figure 1c with two plasmonic Au strip waveguides of equal length (3.5 μm) placed at opposite sides of the junction. The aperiodic groove array was also

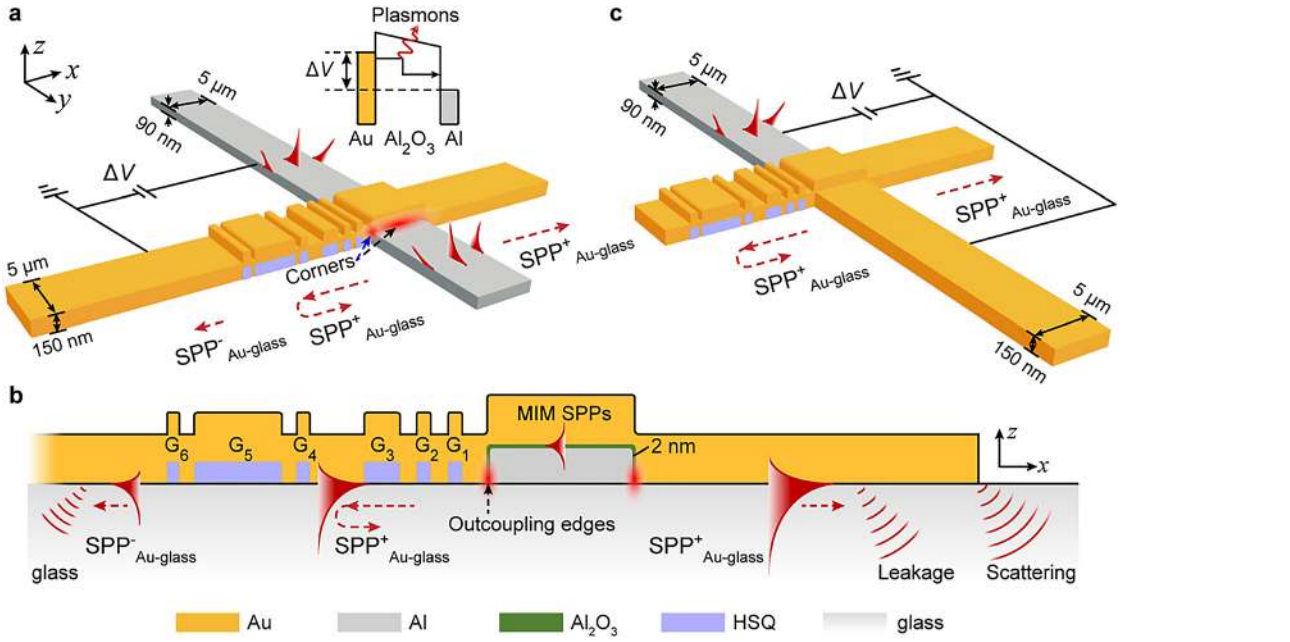

Figure 1: (a) Schematic illustration of the metal–insulator–metal tunnel junction (MIM-TJ) (Al–Al_2O_3–Au) integrated with an aperiodic groove array. Inset: energy-level diagram showing plasmon excitation by inelastic tunneling along with (b) the cross section of the junction. (c) Schematic illustration of the MIM-TJ connected to two 3.5 μm long plasmonic strip waveguides of which on is equipped with an aperiodic groove array.

placed in the $-x$ direction and the thickness of the Al and Au electrodes were 90 and 150 nm, respectively.

3 Optimization of the aperiodic groove array

To optimize the performance of the aperiodic groove array to reflect the $SPP_{Au-glass}$, we used a constrained nonlinear optimization algorithm (sequential quadratic programming, SQP) combined with FDTD simulations (Section S1). Specifically, the objective of the optimization is to maximize P^+ by varying $(w, d) = (w_{G1}, w_{G2}, w_{G3}, w_{G4}, w_{G5}, w_{G6}, d_{G1-G2}, d_{G2-G3}, d_{G3-G4}, d_{G4-G5}, d_{G5-G6})$. Here, the SQP approach guides the objective function at iteration j of the variables (w_j, d_j) by a quasi-Newton's optimization method with Karush–Kuhn–Tucker conditions, then use the minimizer of this subproblem to define a new iteration $j+1$ of the variables (w_{j+1}, d_{j+1}). More details can be referred to the section S1 of the supplementary part. For each of these objective functions, the P^+ value was determined with FDTD calculations until a value of P^+ was found that was higher than the previous iteration; this structure with the high P^+ was then used as the starting point for the next iteration. The aperiodic groove array consists of rectangular-shaped building blocks of equal height (since these structures are easier to fabricate than grooves with varying heights). We used the following constraints of the variables (w, d): the groove height = 40 nm, the total length of the aperiodic array is <3 μm, and the smallest size of the groove width is >50 nm to facilitate fabrication. The step size for the values of (w, d) is 5 nm. We used two-dimensional FDTD simulations to save computing time as shown in Figure 2. In these simulations, the aperiodic groove array was placed on the Au waveguide in the $-x$ direction at a distance of 200 nm from the junction. The dimensions of the junctions (electrode and Al_2O_3 thicknesses) are the same, as shown in Figure 1. To match the experimental geometry, we used a protruded Au aperiodic groove array on top of the Au waveguide but this does not affect the $SPP_{Au-glass}$ mode because of the large thickness of the Au waveguide. The dipole source ($\lambda = 900$ nm) was positioned along the surface normal at the right ($x = -2.5$ μm, $z = 45$ nm) or left ($x = 2.5$ μm, $z = 45$ nm) edge, or center ($x = 0$ μm, $z = 90$ nm), of the junction. Two power monitors were placed at a distance of 3.0 μm away from the edges of the junction to monitor P^- and P^+ and we used the average value of P^+ from the three FDTD calculations with dipole source located in the three different positions. For simplicity, we normalized P^+ as P^+_{Norm} by the power P_0 emitted by the dipole source embedded in the insulator layer (defined in Equation S1).We found that after 30 iterations P^+_{Norm} only increased marginally with subsequent iterations and therefore we stopped the calculation

after 42 iterations when P^{+}_{Norm} reached a value of 41.5 (Figure S2) for an aperiodic groove array with w_{G1} = 70 nm, w_{G2} = 70 nm, w_{G3} = 165 nm, w_{G4} = 68 nm, w_{G5} = 730 nm, w_{G6} = 95 nm, $d_{G1–G2}$ = 160 nm, $d_{G2–G3}$ = 160 nm, $d_{G3–G4}$ = 780 nm, $d_{G4–G5}$ = 160 nm, and $d_{G5–G6}$ = 100 nm. This optimization process is rather efficient as other methods need at least $(N–1) \times 50$ iterations [11]. This method can be, in principle, extended to other frequencies but we limited ourselves to λ = 900 nm since this is close to the maximum of the emitted light from our junctions (see Figure 3c below).

Figure 2 summarizes the FDTD results. Figure 2a shows that the MIM SPP mode is readily excited and propagates along the MIM gap. In this case, the MIM SPP mode fades before it reaches the edge of the junction at the right hand side and therefore it can only outcouple at the left-hand side edge of the junction. The Al and Au electrodes are thick enough to effectively block direct outcoupling of the MIM SPP mode to the metal–air SPP modes. Without the aperiodic groove array, the SPPs propagate along the waveguide in both directions where the value R_e of the $SPP_{Au–glass}$ mode is 0.30 because of absorption by Al and the asymmetrical placement of the dipole (Figure 2a). In sharp contrast, the simulations with the aperiodic groove array placed in the $–x$ direction (Figure 2b) shows that the $SPP^{-}_{Au–glass}$ is efficiently reflected into the $+x$ direction due to the resonance of the localized surface plasmons [11] within the Au grooves (Figure 2c): the value of R_e increases from 0.30 (i.e., small directionality toward the $–x$ direction) to 4.03 (i.e., large directionality to the $+x$ direction). Supporting Information movie 1 shows that the $SPP^{-}_{Au–glass}$ mode is reflected by 180° (which is also apparent from Figure 2b). To prove that this SPP mode is effectively reflected, we also performed simulations with the aperiodic groove array placed 2.2 μm away from the junction. Supplementary material movies 2 shows that $SPP^{-}_{Au–glass}$ mode is indeed reflected by 180°.

Since inelastic tunneling occurs everywhere within the junction area, we calculated the electric field profiles of the SPPs in our optimization process by placing the dipole source also at the center and the right-hand edge of the junction (Figure 2d and e). Considering the incoherent nature of inelastic electron tunneling, we simulated these cases separately to avoid accidental interference of the dipoles. With the dipole source placed at the center, the MIM SPPs still couple to the metal-glass SPP modes although dissipation of the MIM SPPs within the metal–insulator–metal cavity reduces, as expected, the outcoupling efficiency for the simulation with the dipole located to close to the junction edge. The value of R_e is only 7.15 because the field intensities in the aperiodic groove array are low and thus the localized resonances required inside the grooves are also of low intensity and therefore the groove array does not operate well. With the dipole placed at the right-hand edge of the junction, both the

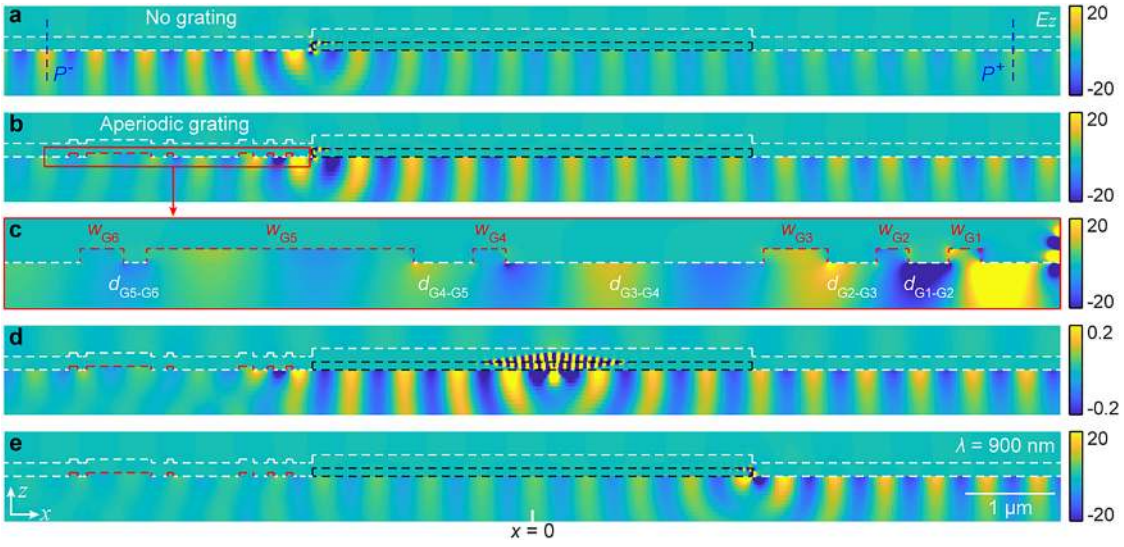

Figure 2: Electric field profile of the surface plasmon polariton (SPP) modes from the metal–insulator–metal tunnel junctions (MIM-TJs) (a) without and (b) with aperiodic groove array placed in the $–x$ direction, where a dipole source was placed at the left edge of the junction. Blue dash lines denote the positions of two monitors to record the power of $SPP^{-}_{Au–glass}$ (P^{-}) and $SPP^{+}_{Au–glass}$ (P^{+}). (c) The enlarged electric field distribution for the aperiodic groove array as indicated by the red rectangle in (b). Electric field profile of the SPPs from the MIM-TJs with aperiodic groove array, where the dipole source was placed at the (d) center and (e) right edge of the junction. x = 0 is located at the center of the junction.

aperiodic groove array and the asymmetric placement of the dipole contribute to the directionality of $SPP_{Au-glass}$ resulting in a very large value of R_e = 44.08. We averaged the extinction ratios for the three specific dipole positions and obtained an overall value of R_e = 18.42 for the optimized aperiodic groove array. This value is high considering the $SPP_{Au-glass}$ mode is reflected by 180°, a much larger angle than what is usually used with optical excitation (where the light source usually illuminates the grooves under an angle of 90° or smaller).

Although the aperiodic groove array was optimized at a single wavelength, it still can work over a broadband of wavelengths because of the intrinsic broad band-gap of the aperiodic grooves [46] and the broadening of the localized resonance modes sustained by the grooves with different widths, which, in turn, is also affected by the number of grooves [11]. To evaluate the spectral response of the aperiodic groove array and the effect of the number of grooves on P^+, we compared the normalized power of the $SPP^+_{Au-glass}$ (P^+_{Norm}, defined in Equation S1) and the $SPP^-_{Au-glass}$ (P^-_{Norm}) as a function of wavelength by adding different groove numbers (3–6) onto the Au waveguide (Figure 3a). The spectra were obtained by averaging the normalized power of three simulations with the dipole source located at the left- and right edge, and at the middle of the junction (Figure S1). As the groove number increases, P^+_{Norm} gradually increases in intensity but this also narrows the full width at half maximum to about 150 nm while the MIM-TJs have rather a broad maximum around 900 nm (Figure 3a). The P^+_{Norm} value only increases 0.02 times at λ = 900 nm when the groove number increases from 5 to 6. To compromise between directionality, the total length of the groove array, and the working bandwidth of the aperiodic groove array, we choose an array of six grooves as the $SPP_{Au-glass}$ reflector.

4 Electrical and optical characterization of the junctions

To experimentally demonstrate the directional excitation of the $SPP_{Au-glass}$ mode, we fabricated the junctions with the aperiodic groove array positioned in the $-x$ (denoted as MIM-TJ$^-$) or $+x$ (MIM-TJ$^+$) direction of the Au waveguide and the symmetrical junction with the array in the $-x$ direction (Section S2). To ensure the mechanism of charge transport across the junctions is quantum mechanical tunneling, we measured the current density–voltage, J(V), characteristics by applying a voltage bias V (in V) to the Al electrode and grounding the Au electrode while measuring the current density J (in μA/cm^2) (Figure 3b, Section S3). The junctions showed a typical exponential increase of J with increasing V and positive parabolic behavior of the dI/dV curves (inset in Figure 3b); these characteristics are associated with off resonant tunneling [47, 48]. We further measured the spectra of photons emitted from the symmetrical junctions and confirmed that the spectra blue shift following the quantum law $h\nu_{photon} \leq e\Delta V$, and the photon emission intensity increases with the applied bias (Figure 3c). These

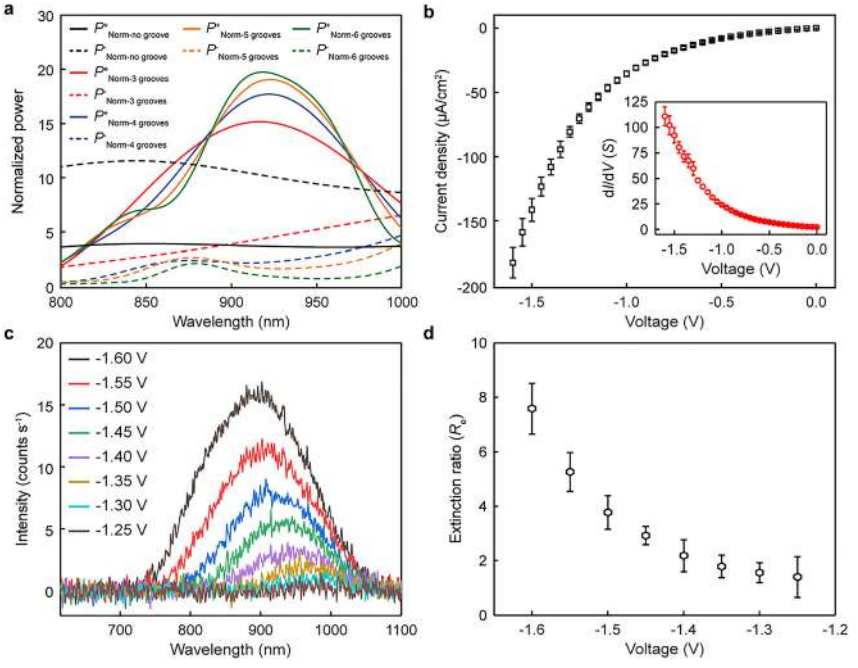

Figure 3: (a) Normalized power of the $SPP^+_{Au-glass}$ and $SPP^-_{Au-glass}$ as a function of wavelength with groove arrays consisting of different numbers of grooves. (b) Current density of the symmetrical junctions as a function of the applied voltages. Inset shows the differential conductance dI/dV of the junctions. Error bars represent the standard deviation determined from six independent tunnel junctions. (c) Spectra measured from the symmetrical junctions at different applied biases. (d) Extinction ratio of the $SPP_{Au-glass}$ under different applied biases. Error bars denote the standard deviation obtained from three different tunnel junctions.

characteristics are typically expected for tunnel junctions where plasmons are excited by inelastic tunneling [20, 49].

Figure 4a–c shows the false-colored scanning electron microscopy (SEM) images of the MIM-TJ$^-$, MIM-TJ$^+$, and the symmetrical junction, respectively. The groove widths of the fabricated aperiodic groove array are slightly (16 nm) larger than that of the theoretically optimized structures which result in a reduction of the performance by a factor of 0.44 at λ = 900 nm (Table 1, Figure S3b). The root mean square (rms) surface roughness of the junctions is 8.2 nm over an area of 1 × 1 μm^2 (Figure S7–8); this roughness facilitates the outcoupling of the MIM SPPs to the $SPP_{Au-glass}$ [39] but has only a minor effect on the propagating of the $SPP_{Au-glass}$ because the bottom surface of the waveguide is determined by the glass substrate.

We used leakage radiation microscopy to characterize the directionality of the plasmon modes from the tunnel junctions. The real and back focal plane (BFP) images were recorded while applying a bias to the junctions using an inverted optical microscope following previously reported methods [20]. Figure 4d–f shows the real plane images of the MIM-TJ$^-$, MIM-TJ$^+$, and the symmetrical junction, respectively, at V = –1.7 V. These images show that photon emission primarily originates from the Al–Au edges of the junction, along with some light scattering from the junction area due to defects induced by the surface roughness of the electrode [41]. Owing to the randomness of the surface roughness and the high confinement of the MIM SPPs, the photons from the junction area are scattered into the far-field over all angles, forming the background signal of the BFP images [50]. From these observations, we conclude that the Al electrode is indeed thick enough to significantly block direct outcoupling of the MIM SPP mode and that this mode primarily outcouples at the edges of the junctions. We also observed light emitted from the ends of the Al and Au strips because of the scattering of the propagating $SPP_{Au-glass}$ and SPP_{Al-air} modes. We note that photons are rarely scattered from the aperiodic groove array, which can be attributed to the low surface roughness of the grooves (Rq = 0.96 nm, Figure S6b) and the weak discontinuity of the permittivity surrounding the groove array (in sharp contrast to the junction edges or the ends of the plasmonic waveguides).

To analyze the SPP modes excited by the tunnel junctions in more detail, we measured the corresponding BFP images from these three junctions at V = –1.7 V (Figure 4g–i) which clearly reveal the directionality of the SPPs characterized by the bright arcs at the right-hand side of the images. For the MIM-TJ$^-$, we observe three bright arc fringes with normalized wavevectors of k/k_0 = 1.49, 1.35, and 1.27 in the $+k_x$ direction of the BFP image, where k_0 is the vacuum wavevector. We attribute these modes to the leakage of the higher-order $SPP_{Au-glass}$ modes as well as to forward scattering at the end of the Au waveguide (Section S5) [51–53]. Similar to the light emitted from the edge of the nanowire [53], scattering of the $SPP_{Au-glass}$ at the end of the Au waveguide propagates into the substrate with an incident angle of θ and projects its wavevector onto the Fourier plane as $k = \sqrt{k_x^2 + k_y^2} = nk_0\sin\theta$, where n is the refractive index of the substrate. In addition, the weak arc at k/k_0 = 1.02 corresponds to the scattering of the SPP_{Au-air} mode at the end of the Au waveguide. Since the Au waveguide in the $-x$ direction connects to Au pad and has no end of the waveguide for SPP scattering, we only observed one weak fringe of the leakage of $SPP_{Au-glass}$ with $k/k_0 = -1.33$ at the $-k_x$ direction of the BFP image. Although we optimized the aperiodic groove array for the reflection of $SPP_{Au-glass}$ by 180° under normal incidence, the $SPP_{Au-glass}$ modes can propagate along varying angles in the x direction because of the finite width of the Au waveguide. Therefore, these $SPP_{Au-glass}$ modes detected by the BFP images result in an arc feature with a wavevector of $k = \sqrt{k_x^2 + k_y^2}$. We extracted the fringes from the two sides of the BFP images and obtained an extinction ratio of R_e = 12.53 using Equation (1) (Section S7), which is comparable to the overall average value of 18.42 calculated by FDTD simulations. Note that the scattered photons from the junction edges and the junction area diffuse into the background in the BFP images [41, 50].

Interestingly, a horizontal line with $k_y/k_0 \approx 1$ and a vertical line with $k_x/k_0 \approx -1$ were observed in the BFP image (indicated by the ochre dashed arrows in Figure 4g). These two straight lines originate from the conical edge diffraction of a one-dimensional SPP_{Al-air} and SPP_{Au-air} mode propagating along the 90° edges of the Al and Au strip waveguides, respectively, similar to observations reported by Bouhelier and coworkers [54, 55]. These modes are outcoupled from the top corners of the junction, as indicated by the blue dash arrow in Figure 1a. Moreover, we observed two bright arcs located at the upper and lower side of the BFP image near the inner circle of k/k_0 = 1 (indicated by the gray dashed arrows in Figure 4g). The upper arc corresponds to the scattering of the SPP_{Al-air} at the boundary of the top surface of the Al waveguide, and the lower arc is the scattering of the SPP_{Al-air} at the end of the Al waveguide [56].

For the MIM-TJ$^+$, however, we only observe one distinct leakage mode with k/k_0 = 1.35 in the $+k_x$ side of the BFP image (Figure 4h) because of the reflection of $SPP^+_{Au-glass}$ by the aperiodic groove array. Compared with the BFP

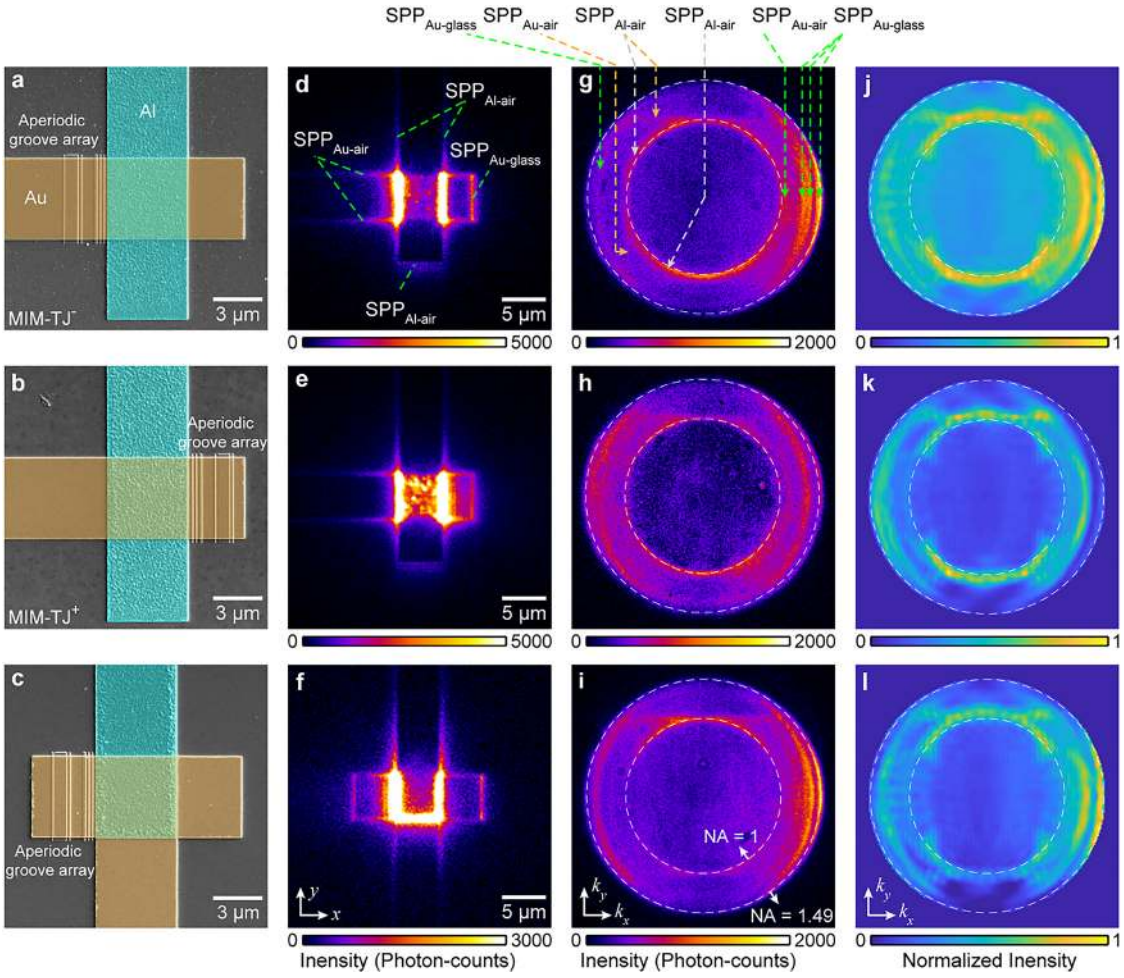

Figure 4: (a)–(c) False-colored scanning electron microscopy (SEM) images of the metal–insulator–metal tunnel junctions (MIM-TJ$^-$, MIM-TJ$^+$), and the junction connecting two Au waveguides. (d)–(f) The corresponding real plane images, (g)–(i) the measured, and (j)–(l) simulated back focal plane (BFP) images of the MIM-TJ$^-$, MIM-TJ$^+$, and the symmetrical junction under the applied bias of $V = -1.7$ V.

image of MIM-TJ$^-$, the arc fringe located at $k/k_0 = 1.49$ completely disappeared because only a fraction (18.6% according to the simulations described earlier) of the $SPP^+_{Au-glass}$ mode crosses the aperiodic groove array and reaches the end of the waveguide. Moreover, since the waveguide at the left-hand side is connected to the pad, most of the SPP modes propagating to the $-x$ direction, including the $SPP^-_{Au-glass}$ and the reflected $SPP^+_{Au-glass}$, dissipate due to absorption by Au. Therefore, we observed similar intensities in the left and right sides of the BFP image of the MIM-TJ$^+$. Similarly, we obtained the $R_e = 1.20$ based on the fringes on both sides of the BFP images, which is much lower than the value of the MIM-TJ$^+$, $R_e = 12.53$ because of the reflection of the $SPP_{Au-glass}$ mode by the aperiodic groove array. Considering the asymmetry of the junction and the inherent differences between the MIM-TJ$^+$ and MIM-TJ$^-$, we measured the BFP images of the symmetrical junction to directly quantify the directionality of the SPP modes. Figure 4i shows the BFP image of the symmetrical junction where the $SPP_{Au-glass}$ mode with $k/k_0 = 1.49$, 1.38, and 1.30 in the $+k_x$ direction is clearly visible. In contrast, only one weak fringe ($k/k_0 = 1.39$) can be observed in the $-k_x$ direction. In addition, the conical edge diffraction (horizontal line, $k_y/k_0 \approx 1.0$) and the boundary scattering (upper arch) of the SPP_{Al-air} propagating along the top surface of Al waveguide are also visible. The three-dimensional FDTD simulations (Section S6) confirm the directional excitation of the $SPP_{Au-glass}$ mode resulting in an asymmetrical BFP image (Figure 4j–l). Therefore, we experimentally demonstrated that the aperiodic groove array reflects the $SPP_{Au-glass}$ and, consequently, scattering at the end of the waveguide is diminished.

5 Directionality of the $SPP_{Au-glass}$

The MIM-TJs$^+$ and MIM-TJs$^-$ made it possible to determine that the $SPP_{Au-glass}$ mode was reflected by the aperiodic groove array, but these junctions do not allow to experimentally determine the directionality induced solely by the aperiodic groove array due to other asymmetries present in these structures. We obtained the extinction ratio R_e of the $SPP_{Au-glass}$ from the measured BFP images of the symmetrical junctions as shown in Figure 2d. The R_e gradually increases as we increased the applied bias because the plasmon emission intensity increases and the maximum of the broad spectra blue shift to $\lambda = 900$ nm. The value of R_e of 7.59 ± 0.93 at $V = -1.6$ V was obtained from three independent junctions. This value is lower than the calculated R_e value of 18.42 due to losses induced by, e.g., surface roughness of the electrodes, but also due to the fact that the calculations only consider $\lambda = 900$ nm while the junctions excite plasmons with varying frequencies. Compared with a light-emitting diode (LED) based plasmon source equipped with an asymmetrical grating (where photons reach the grating along the surface normal) with directionality of 10 [57], our measured extinction ratio of $R_e \approx 8$ is considerable because of the large momentum mismatch between the MIM SPP mode and the single interface SPP modes and our grating reflects the $SPP_{Au-glass}$ mode by 180°.

6 Conclusion

In summary, we achieved directional SPP excitation from Al–Al_2O_3–Au tunnel junctions by integrating an aperiodic groove array into Au waveguides. The tunnel junctions excite all available modes including high-order $SPP_{Au-glass}$, SPP_{Au-air}, SPP_{Al-air} as well as one-dimensional edge mode that are otherwise difficult to access by optical means. This electrically driven aperiodic groove array designed by new and efficient nonlinear optimization algorithms reflects the $SPP_{Au-glass}$ mode by 180° with a maximum directionality of $R_e = 7.59 \pm 0.93$. Although this value is smaller than that typically obtained with optically driven gratings (which are usually excited with narrowband sources, such as, lasers), this value is remarkable given the broadband nature of SPP excitation by planar tunnel junctions. The directionality of $SPP_{glass-Au}$ from experimental results is smaller than the simulated averaged value of 18.42. Therefore, our results suggest that there is plenty of room for improvements by narrowing the spectral bandwidth of the plasmon source and reducing the roughness of the electrode materials.

7 Methods

7.1 Numerical simulation

We used a seamless coupling Matlab-driven optimization mechanism (constrained nonlinear optimization algorithms) connected with Lumerical solver (FDTD solutions) to design and optimize the aperiodic groove array as explained in the main text and more details are provided in Supplementary Section 1.

The numerical calculations of the electric field distributions were performed using two-dimensional FDTD simulations with a MIM-TJ with a 90-nm-thick and 5-μm-wide Al bottom electrode, 2-nm-thick Al_2O_3 layer, and a 150-nm thick, infinitely long Au top electrode. The optimized aperiodic groove array has the following dimensions: $w_{G1} = 70$ nm, $w_{G2} = 70$ nm, $w_{G3} = 165$ nm, $w_{G4} = 68$ nm, $w_{G5} = 730$ nm, $w_{G6} = 95$ nm, distance $d_{G1-G2} = 160$ nm, $d_{G2-G3} = 160$ nm, $d_{G3-G4} = 780$ nm, $d_{G4-G5} = 160$ nm, and $d_{G5-G6} = 100$ nm, and height $h = 40$ nm. This groove array was placed at 200 nm from the left edge of the junction. The optical properties of the Al and Au were taken from Palik's handbook, the reflective index of glass, Al_2O_3, and HSQ of the aperiodic groove array were 1.52, 1.8, and 1.4, respectively [58]. A dipole was placed at three specific positons (top center, left center, and right center of the insulator layer) to excite the SPP modes. Two monitors were placed at 3.0 μm from the two edges of the junctions to record the power flows to $+x$ (P^+) and $-x$ (P^-) directions. The results are shown in Figure 2.

The numerical calculations of the BFP images were performed using the near field to far field transformation method. The near field was obtained from the FDTD simulations where different SPP modes were scattered or leaked into the glass substrate at different angles. We discarded the SPP modes with wavevectors $k/k_0 > \text{NA} = 1.49$ and focused the remaining modes into the image plane to form the BFP images. The details of these calculations are provided in Supplementary Sections S6, and the results are given in Figure 4.

7.2 Sample fabrication

The Au–Al_2O_3–Au tunnel junctions were fabricated on borosilicate coverslips with a refractive index of 1.52 and a thickness of 0.17 mm. The HSQ aperiodic groove array with a thickness of 40 nm was fabricated using electron-beam lithography (JEOL, JBX-6300FS). Both the Au and Al electrodes were also fabricated using electron-beam lithography and followed by electron beam deposition (AJA Ebeam Evaporator) and liftoff process. The details of the fabrication process are provided in Supplementary Section 2.

7.3 Electrical characterization

The electrical characterization of the MIM-TJs was performed using a source meter (Keithley 6430, Keithley Instruments) with a guard and noise shield. The source meter was controlled by home-made Labview software to provide the applied voltage and record the corresponding current.

7.4 Optical characterization

The optical characterization of the MIM-TJs was performed using a wide-field inverted optical microscope (Nikon Eclipse Ti-E) with an oil

objective (magnification ×100, numerical aperture NA = 1.49). An Andor EMCCD (electron-multiplying charge coupled device, iXon Ultra 897) was used for the real plane and BFP imaging, and an Andor spectrometer (Shamrock 303i) was used for the spectral measurements. We measured the spectra from the entire device including the junction edges, junction area, and the edges of the waveguides, through the glass substrate and the spectra have been corrected by the quantum efficiency of our detector.

Acknowledgment: We acknowledge the National Research Foundation (NRF) for supporting this research under Prime Minister's Office, Singapore under its Medium sized centre programme, and the Competitive Research Programme (CRP) program (NRF-CRP17-2017-08).

Author contributions: All the authors have accepted responsibility for the entire content of this submitted manuscript and approved submission.

Research funding: This research was funded by the Competitive Research Programme (CRP) program (NRF-CRP17-2017-08).

Conflict of interest statement: The authors declare no conflicts of interest regarding this article.

References

[1] W. L. Barnes, A. Dereux, and T. W. Ebbesen, "Surface plasmon subwavelength optics," *Nature*, vol. 424, pp. 824–830, 2003.

[2] Y. Fu and X. Zhou, "Plasmonic lenses: a review," *Plasmonics*, vol. 5, pp. 287–310, 2010.

[3] A. G. Brolo, "Plasmonics for future biosensors," *Nat. Photonics*, vol. 6, pp. 709–713, 2012.

[4] Y. Fang and M. Sun, "Nanoplasmonic waveguides: towards applications in integrated nanophotonic circuits," *Light Sci. Appl.*, vol. 4, pp. e294–e294, 2015.

[5] D. Wang, W. Wang, M. P. Knudson, G. C. Schatz, and T. W. Odom, "Structural engineering in plasmon nanolasers," *Chem. Rev.*, vol. 118, pp. 2865–2881, 2018.

[6] H. A. Atwater and A. Polman, "Plasmonics for improved photovoltaic devices," *Nat. Mater.*, vol. 9, pp. 205–213, 2010.

[7] D. K. Gramotnev and S. I. Bozhevolnyi, "Plasmonics beyond the diffraction limit," *Nat. Photonics*, vol. 4, pp. 83–91, 2010.

[8] A. V. Zayats, I. I. Smolyaninov, and A. A. Maradudin, "Nano-optics of surface plasmon polaritons," *Phys. Rep.*, vol. 408, pp. 131–314, 2005.

[9] A. Pors, M. G. Nielsen, T. Bernardin, J.-C. Weeber, and S. I. Bozhevolnyi, "Efficient unidirectional polarization-controlled excitation of surface plasmon polaritons," *Light Sci. Appl.*, vol. 3, pp. e197–e197, 2014.

[10] W. Yao, S. Liu, H. Liao, et al., "Efficient directional excitation of surface plasmons by a single-element nanoantenna," *Nano Lett.*, vol. 15, pp. 3115–3121, 2015.

[11] X. Huang and M. L. Brongersma, "Compact aperiodic metallic groove arrays for unidirectional launching of surface plasmons," *Nano Lett.*, vol. 13, pp. 5420–5424, 2013.

[12] A. Baron, E. Devaux, J. C. Rodier, et al., "Compact antenna for efficient and unidirectional launching and decoupling of surface plasmons," *Nano Lett.*, vol. 11, pp. 4207–4212, 2011.

[13] M. U. González, J. C. Weeber, A. L. Baudrion, et al., "Design, near-field characterization, and modeling of 45° surface-plasmon Bragg mirrors," *Phys. Rev. B*, vol. 73, p. 155416, 2006.

[14] T. J. Davis, D. E. Gómez, and A. Roberts, "Plasmonic circuits for manipulating optical information," *Nanophotonics*, vol. 6, pp. 543–559, 2017.

[15] B. Schwarz, P. Reininger, D. Ristanic, et al., "Monolithically integrated mid-infrared lab-on-a-chip using plasmonics and quantum cascade structures," *Nat. Commun.*, vol. 5, p. 4085, 2014.

[16] J. Lambe and S. L. McCarthy, "Light emission from inelastic electron tunneling," *Phys. Rev. Lett.*, vol. 37, pp. 923–925, 1976.

[17] S. L. McCarthy and J. Lambe, "Enhancement of light emission from metal-insulator-metal tunnel junctions," *Appl. Phys. Lett.*, vol. 30, pp. 427–429, 1977.

[18] J. Kirtley, T. N. Theis, and J. C. Tsang, "Light emission from tunnel junctions on gratings," *Phys. Rev. B*, vol. 24, pp. 5650–5663, 1981.

[19] M. Parzefall, P. Bharadwaj, A. Jain, T. Taniguchi, K. Watanabe, and L. Novotny, "Antenna-coupled photon emission from hexagonal boron nitride tunnel junctions," *Nat. Nanotechnol.*, vol. 10, pp. 1058–1063, 2015.

[20] W. Du, T. Wang, H.-S. Chu, and C. A. Nijhuis, "Highly efficient on-chip direct electronic–plasmonic transducers," *Nat. Photonics*, vol. 11, pp. 623–627, 2017.

[21] D. Shafir, H. Soifer, B. D. Bruner, et al., "Resolving the time when an electron exits a tunnelling barrier," *Nature*, vol. 485, pp. 343–346, 2012.

[22] G. Walter, C. H. Wu, H. W. Then, M. Feng, and N. Holonyak Jr., "4.3 GHz optical bandwidth light emitting transistor," *Appl. Phys. Lett.*, vol. 94, p. 241101, 2009.

[23] L. C. Davis, "Theory of surface-plasmon excitation in metal-insulator-metal tunnel junctions," *Phys. Rev. B*, vol. 16, pp. 2482–2490, 1977.

[24] H. Qian, S.-W. Hsu, K. Gurunatha, et al., "Efficient light generation from enhanced inelastic electron tunnelling," *Nat. Photonics*, vol. 12, pp. 485–488, 2018.

[25] F. Bigourdan, J. P. Hugonin, F. Marquier, C. Sauvan, and J. J. Greffet, "Nanoantenna for electrical generation of surface plasmon polaritons," *Phys. Rev. Lett.*, vol. 116, p. 106803, 2016.

[26] J. Kern, R. Kullock, J. Prangsma, M. Emmerling, M. Kamp, and B. Hecht, "Electrically driven optical antennas," *Nat. Photonics*, vol. 9, pp. 582–586, 2015.

[27] X. He, J. Tang, H. Hu, et al., "Electrically driven highly tunable cavity plasmons," *ACS Photonics*, vol. 6, pp. 823–829, 2019.

[28] C. Zhang, J. P. Hugonin, A. L. Coutrot, C. Sauvan, F. Marquier, and J. J. Greffet, "Antenna surface plasmon emission by inelastic tunneling," *Nat. Commun.*, vol. 10, p. 4949, 2019.

[29] M. Parzefall and L. Novotny, "Optical antennas driven by quantum tunneling: a key issues review," *Rep. Prog. Phys.*, vol. 82, p. 112401, 2019.

[30] S. P. Gurunarayanan, N. Verellen, V. S. Zharinov, et al., "Electrically driven unidirectional optical nanoantennas," *Nano Lett.*, vol 17, pp. 7433–7439, 2017.

[31] R. Kullock, M. Ochs, P. Grimm, M. Emmerling, and B. Hecht, "Electrically-driven Yagi-Uda antennas for light," *Nat. Commun.*, vol. 11, p. 115, 2020.
[32] J.-G. Zhu and C. Park, "Magnetic tunnel junction," *Mater. Today*, vol. 9, pp. 36–45, 2006.
[33] C. A. Reynaud, D. Duché, J. J. Simon, et al., "Rectifying antennas for energy harvesting from the microwaves to visible light: a review," *Prog. Quan. Electron.*, vol. 72, p. 100265, 2020.
[34] S. Krishnan, H. La Rosa, E. Stefanakos, S. Bhansali, and K. Buckle, "Design and development of batch fabricatable metal–insulator–metal diode and microstrip slot antenna as rectenna elements," *Sens. Actuators. A. Phys.*, vol. 142, pp. 40–47, 2008.
[35] S. Krishnan, S. Bhansali, E. Stefanakos, and Y. Goswami, "Thin film metal-insulator-metal junction for millimeter wave detection," *Procedia Chem.*, vol. 1, pp. 409–412, 2009.
[36] A. M. Ionescu and H. Riel, "Tunnel field-effect transistors as energy-efficient electronic switches," *Nature*, vol. 479, pp. 329–337, 2011.
[37] E. N. Grossman, T. E. Harvey, and C. D. Reintsema, "Controlled barrier modification in Nb/NbOx/Ag metal insulator metal tunnel diodes," *J. Appl. Phys.*, vol. 91, pp. 10134–10139, 2002.
[38] G. Droulers, S. Ecoffey, M. Pioro-Ladrière, and D. Drouin, "Effects of aging on nanoscale planar metal-insulator-metal tunnel junctions," *J. Vac. Sc. Technol. B*, vol. 34, p. 062203, 2016.
[39] J. B. D. Soole and H. P. Hughes, "Roughness-coupled light emission from tunnel junctions: the role of the fast surface plasmon," *Surf. Sci.*, vol. 197, 250–266, 1988.
[40] M. Parzefall and L. Novotny, "Light at the end of the tunnel," *ACS Photonics*, vol 5, pp. 4195–4202, 2018.
[41] K. S. Makarenko, T. X. Hoang, T. J. Duffin, et al., "Efficient surface plasmon polariton excitation and control over outcoupling mechanisms in metal–insulator–metal tunneling junctions," *Adv. Sci.*, vol. 7, p. 1900291, 2020.
[42] H. Liu and P. Lalanne, "Light scattering by metallic surfaces with subwavelength patterns," *Phys. Rev. B*, vol. 82, p. 115418, 2010.
[43] B. Wang and P. Lalanne, "How many surface plasmons are locally excited on the ridges of metallic lamellar gratings?" *Appl. Phys. Lett.*, vol. 96, p. 051115, 2010.
[44] S. Molesky, Z. Lin, A. Y. Piggott, W. Jin, J. Vucković, and A. W. Rodriguez, "Inverse design in nanophotonics," *Nat. Photonics*, vol. 12, pp. 659–670, 2018.
[45] S. G. Rodrigo, F. J. García-Vidal, and L. Martín-Moreno, "Influence of material properties on extraordinary optical transmission through hole arrays," *Phys. Rev. B*, vol. 77, p. 075401, 2008.
[46] J. S. Bouillard, S. Vilain, W. Dickson, G. A. Wurtz, and A. V. Zayats, "Broadband and broadangle SPP antennas based on plasmonic crystals with linear chirp," *Sci. Rep.*, vol. 2, p. 829, 2012.
[47] J. G. Simmons, "Electric tunnel effect between dissimilar electrodes separated by a thin insulating film," *J. Appl. Phys.*, vol. 34, pp. 2581–2590, 1963.
[48] W. F. Brinkman, R. C. Dynes, and J. M. Rowell, "Tunneling conductance of asymmetrical barriers," *J. Appl. Phys.*, vol. 41, pp. 1915–1921, 1970.
[49] K. Parvin and W. Parker, "Optical spectra and angular dependence of the visible light emitted by metal-insulator-metal tunnel junctions," *Solid State Comm.*, vol. 37, pp. 629–633, 1981.
[50] N. Cazier, M. Buret, A. V. Uskov, et al., "Electrical excitation of waveguided surface plasmons by a light-emitting tunneling optical gap antenna," *Opt. Express*, vol. 24, pp. 3873–3884, 2016.
[51] R. Zia, M. D. Selker, and M. L. Brongersma, "Leaky and bound modes of surface plasmon waveguides," *Phys. Rev. B*, vol. 71, p. 165431, 2005.
[52] V. A. Zenin, R. Malureanu, I. P. Radko, A. V. Lavrinenko, and S. I. Bozhevolnyi, "Near-field characterization of bound plasmonic modes in metal strip waveguides," *Opt. Express*, vol. 24, pp. 4582–4590, 2016.
[53] T. Shegai, V. D. Miljkovic, K. Bao, et al., "Unidirectional broadband light emission from supported plasmonic nanowires," *Nano Lett.*, vol. 11, pp. 706–711, 2011.
[54] J. Berthelot, F. Tantussi, P. Rai, et al., "Determinant role of the edges in defining surface plasmon propagation in stripe waveguides and tapered concentrators," *J. Opt. Soc. Am. B*, vol. 29, pp. 226–231, 2012.
[55] J. Berthelot, A. Bouhelier, G. C. d. Francs, J.-C. Weeber, and A. Dereux, "Excitation of a one-dimensional evanescent wave by conical edge diffraction of surface plasmon," *Opt. Express*, vol. 19, pp. 5303–5312, 2011.
[56] G. Beane, K. Yu, T. Devkota, et al., "Surface plasmon polariton interference in gold nanoplates," *J. Phys. Chem. Lett.*, vol. 8, pp. 4935–4941, 2017.
[57] L. Wang, T. Li, L. Li, W. Xia, X. G. Xu, and S. N. Zhu, "Electrically generated unidirectional surface plasmon source," *Opt. Express*, vol. 20, pp. 8710–8717, 2012.
[58] E. D. Palik, *Handbook of Optical Constants of Solids*, Orlando, Academic Press, 1985.

Supplementary Material: The online version of this article offers supplementary material (https://doi.org/10.1515/nanoph-2020-0558).